Ultrahigh resolution Fourier domain optical coherence tomography

R. A. Leitgeb[1], W. Drexler[1,2], A. Unterhuber[1,2], B. Hermann[1,2], T. Bajraszewski[3], T. Le[4], A. Stingl[4], and A. F. Fercher[1]

[1]Department of Medical Physics, Medical University of Vienna, Waehringerstrasse 13, A-1090 Vienna, Austria
[2]Chrisitan Doppler Laboratory, Medical University of Vienna, Waehringerstrasse 13, A-1090 Vienna, Austria
[3]Institute of Physics, Nicholas Copernicus University, Grudziadzka 5/7, Pl-87100, Torun, Poland
[4] Femtolaser Produktions GmbH, Fernkorngasse 10, A-1100 Vienna, Austria

rainer.leitgeb@meduniwien.ac.at

Abstract: We present, for the first time, *in vivo* ultrahigh resolution (~2.5 µm in tissue), high speed (10000 A-scans/second equivalent acquisition rate sustained over 160 A-scans) retinal imaging obtained with Fourier domain (FD) OCT employing a commercially available, compact (500x260mm), broad bandwidth (120 nm at full-width-at-half-maximum centered at 800 nm) Titanium:sapphire laser (Femtosource Integral OCT, Femtolasers Produktions GmbH). Resolution and sampling requirements, dispersion compensation as well as dynamic range for ultrahigh resolution FD OCT are carefully analyzed. *In vivo* OCT sensitivity performance achieved by ultrahigh resolution FD OCT was similar to that of ultrahigh resolution time domain OCT, although employing only 2-3 times less optical power (~300 µW). Visualization of intra-retinal layers, especially the inner and outer segment of the photoreceptor layer, obtained by FDOCT was comparable to that, accomplished by ultrahigh resolution time domain OCT, despite an at least 40 times higher data acquisition speed of FD OCT.

OCIS codes: (170.4500) optical coherence tomography, (120.3890) medical optics instrumentation, (170.4580) optical diagnostics for medicine, (140.3590) Lasers, titanium.

References and Links

1. D. Huang, E. A. Swanson, C. P. Lin, J. S. Schuman, W. G. Stinson, W. Chang, M. Hee, T. Flotte, K. Gregory, C. A. Puliafito, and J. G. Fujimoto, "Optical coherence tomography," Science **254**, 1178-1181 (1991).
2. W. Drexler, "Ultrahigh resolution optical coherence tomography," J. Biomed. Opt. **9**, 47-74 (2004).
3. W. Drexler, H. Sattmann, B. Hermann, T.H. Ko, M. Stur, A. Unterhuber, C. Scholda, O. Findl, M. Wirtitsch, J.G. Fujimoto, and A. F. Fercher, "Enhanced visualization of macular pathology using ultrahigh resolution optical coherence tomography," *Arch. Ophthalmol*. **121**, 695-706, (2003).
4. A. M. Rollins, M. D. Kulkarni, S. Yazdanfar, R. Ung-arunyawee, and J. A. Izatt, "In vivo video rate optical coherence tomography," Opt. Express **3** , 219 (1998). http://www.opticsexpress.org/abstract.cfm?URI=OPEX-3-6-219.
5. A. F. Fercher, C. K. Hitzenberger, G. Kamp, and S. Y. El-Zaiat, "Measurement of intraocular distances by backscattering spectral interferometry," Optics Communications **117**, 43-48 (1995).
6. M. Wojtkowski, R.Leitgeb, A. Kowalczyk, T. Bajraszewski, and A.F.Fercher, "In-vivo human retinal imaging by Fourier domain optical coherence tomography," J. Biomed. Opt. **7**, 457-463 (2002).
7. T. Mitsui, "Dynamic Range of Optical Reflectometry with Spectral Interferometry," Jpn. J. Appl. Phys. **38**, 6133-6137 (1999).
8. P. Andretzky, M. Knauer, F. Kiesewetter, and G. Haeusler, "Optical Coherence Tomography by Spectral Radar: Improvement of Signal-to-Noise Ratio," Proc. SPIE 3915, 55-59 (2000).
9. R. A. Leitgeb, C. K. Hitzenberger, and A. F. Fercher, "Performance of Fourier domain vs. time domain optical coherence tomography," Optics Express **11**, 889-894 (2003). http://www.opticsexpress.org/abstract.cfm?URI=OPEX-11-8-889.
10. M. A. Choma, M. V. Sarunic, C. Yang, and J. A. Izatt, "Sensitivity advantage of swept source and Fourier domain optical coherence tomography," Opt. Expr. **11**, 2183 (2003) http://www.opticsexpress.org/abstract.cfm?URI=OPEX-11-18-2183.

#4012 - $15.00 US Received 11 March 2004; revised 28 April 2004; accepted 3 May 2004

11. J. F. De Boer, B. Cense, B. H. Park, M. C. Pierce, G. J. Tearney, and B. E. Bouma, "Improved signal-to-noise ratio in spectral-domain compared with time-domain optical coherence tomography," Opt. Lett. **28**, 2067-2069 (2003).
12. N. Nassif, B. Cense, B. H. Park, S. H. Yun, T. C. Chen, B. E. Bouma, G. J. Tearney, and J. F. de Boer, "In vivo human retinal imaging by ultrahigh-speed spectral domain optical coherence tomography," Opt. Lett. **29**, 480-482 (2004).
13. S. H. Yun, G. J. Tearney, B. E. Bouma, B. H. Park, and J. F. de Boer," High-speed spectral-domain optical coherence tomography at 1.3 µm wavelength," Opt. Express **11**, 3598-3604 (2003). http://www.opticsexpress.org/abstract.cfm?URI=OPEX-11-26-3598.
14. N. A. Nassif, B. Cense, B. H. Park, M. C. Pierce, S. H. Yun, B. E. Bouma, G. J. Tearney, T. C. Chen, and J. F. de Boer, "In vivo high-resolution video-rate spectral-domain optical coherence tomography of the human retina and optic nerve," Optics Express **12**, 367-376 (2004) http://www.opticsexpress.org/abstract.cfm?URI=OPEX-11-25-3490.
15. R. Leitgeb, L. Schmetterer, F. Berisha, C. K. Hitzenberger, M. Wojtkowski, T. Bajraszewski, and A. F. Fercher, "Real- time measurements of in-vitro flow by Fourier domain optical coherence tomography," Opt. Lett. **29**, 171-174 (2004) .
16. R. A. Leitgeb, L. Schmetterer, W. Drexler, T. Bajraszewski, R. J. Zawadzki, and A. F. Fercher, "Real-time assessment of retinal blood flow with ultrafast acquisition by color Doppler Fourier domain optical coherence tomography," Optics Express **11**, 3116 (2003); http://www.opticsexpress.org/abstract.cfm?URI=OPEX-11-23-3116 .
17. B. R. White, M. C. Pierce, N. Nassif, B. Cense, B. H. Park, G. J. Tearney, B. E. Bouma, T. C. Chen, and J. F. de Boer, "In vivo dynamic human retinal blood flow imaging using ultra-high-speed spectral domain optical coherence tomography," Opt. Expr. **11**, 3490 (2003) http://www.opticsexpress.org/abstract.cfm?URI=OPEX-11-25-3490.
18. M.Wojtkowski, A. Kowalczyk, R. Leitgeb, and A. F.Fercher, "Full range complex spectral optical coherence tomography," Opt. Lett. **27**, 1415-1418 (2002).
19. R. A. Leitgeb, C.K. Hitzenberger, T. Bajraszewski, and A. F. Fercher, "Phase shifting method to achieve high speed long depth range imaging using FDOCT," Opt. Lett. **28**, 2201-2204 (2003).
20. C.K. Hitzenberger, A. Baumgartner, W. Drexler, and A. F. Fercher, "Dispersion effects in partial coherence interferometry: Implications for intraocular ranging," J. Biomed. Opt. **4**, 144-151 (1999).
21. W.Drexler, B. Hermann, A. Unterhuber, H. Sattmann, T. H. Ko, M. Wirtitsch, M. Stur, C. Scholda, E. Ergun, A. Anger, P.Ahnelt, J. G.Fujimoto, and A. F. Fercher, "Quantification of photoreceptor layer thickness in different macular pathologies using ultra high resolution optical coherence tomography," SPIE Proc. **5214**, 5214-27 (2004).

1. Introduction

Optical coherence tomography (OCT) is already a well established biomedical imaging technique due to its outstanding axial resolution [1]. It is a basic principle of coherent optics that the axial or temporal resolution is inverse proportional to the optical bandwidth of the used partially coherent light source. The development of new ultrabroad bandwidth light sources enabled ultrahigh resolution OCT (UHR OCT) [2]. With the enhanced axial resolution of 3µm and below it is nowadays possible to obtain in vivo OCT tomograms close to the level of histology. In clinical practice, the visualization of subtle morphological features has improved the early diagnosis and the assessment of tissue pathologies [3]. Current ultrahigh resolution systems perform visualization of tissue microstructure in the so-called time domain. Depth information in this case is obtained as a function of distance or time. In time domain OCT it is essentially the relative optical path length in a Michelson interferometer between reference mirror and sample structure that is changed with time. Sophisticated depth scanning devices have been implemented to provide high scanning speeds of up to 8 kHz, i.e., 8000 A-scans per second [4]. However the drawback of faster scanning speed and longer depth range in time domain is lower system sensitivity. During the last year an alternative OCT method caught the attention of the biomedical imaging community: Fourier domain OCT (FD OCT)[5-19]. The whole depth structure (A-scan) is obtained synchronously and no depth scanning is necessary. The acquisition speed is only limited by the read out rate of the CCD camera that records the backscattered light intensity as a function of frequency rather than time. Due to the decoupling of scanning range and electronic detection band width, FD OCT enables a significant sensitivity advantage that allows increasing the line rate (A-scan rate) without loosing imaging performance in comparison to TD OCT [7-11]. Hence the achievable

#4012 - $15.00 US Received 11 March 2004; revised 28 April 2004; accepted 3 May 2004

high speed imaging performance allows three dimensional tissue visualization [14] as well as to study *in vivo* functional tissue properties like perfusion and vessel pulsatility [15-17].

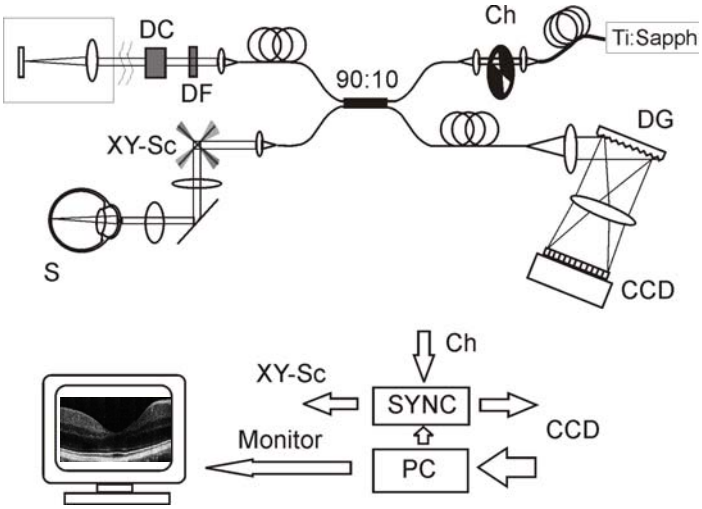

Fig. 1. Schematic of the ultrahigh resolution FD OCT system: Ti:Sapp, broad bandwidth Titanium:sapphire laser (Femtosource Integral OCT); Ch, Chopper wheel; DF, neutral density filter; DC, dispersion control; DG, diffraction grating; X-Y-Sc, transverse galvo scanners; S, sample; SYNC, microelectronics for synchronizing system components; PC, personal computer; CCD, charge coupled device.

2. Methods

2.1. Experimental setup

The setup of the ultrahigh resolution FD OCT system is depicted in Fig. 1. The light source is a recently developed compact (500x260mm) femtosecond pulsed Titanium:sapphire laser (Femtosource Integral OCT; Femtolasers Produktions GmbH., Austria) with a spectral bandwidth of 120nm (full-width-at-half-maximum: FWHM) centered at 800nm and ~40 mW ex fiber output power . The laser output was coupled into a 100 meter long optic fiber which was used to provide dispersive stretching of the pulse duration to hundreds of picoseconds. This reduces the peak pulse intensities by several orders of magnitude and since the laser operates at an 80 MHz repetition rate, the output can be treated as continuous wave The chopper at the entrance of the fiber based Michelson interferometer avoids light exposure of the CCD and the sample during the read out cycle of the CCD and the data transfer to the PC. It also supplies the trigger signal for the system synchronization. The light is split via a 2x2 fiber coupler (90:10) into reference and sample arm light. In the sample arm we used the scanning head of a modified commercially available OCT 1 system (Carl Zeiss Meditec Inc., Dublin, CA) that was adapted for broadband light. In the reference arm the light is reflected from a static silver mirror. The neutral density filter is adjusted to yield a light level on the CCD that provides shot noise limited detection. This is done by gradually increasing the reference arm level until the sensitivity reaches its maximal value, in our case at 80% of the CCD saturation level with 3mW at the reference arm fiber output. Further increase leads to a sensitivity decay which is due to increasing RIN noise as well as the increased incoherent background light. If RIN noise dominated for all reference powers one could not reach a maximum sensitivity. The sensitivity would always decrease with increasing reference arm light. The dispersion needs to be handled with great care and is balanced via BK7 and 25-27mm of water in the reference arm. The latter one mainly compensates dispersion mismatch

#4012 - $15.00 US Received 11 March 2004; revised 28 April 2004; accepted 3 May 2004

introduced by the ocular media. The polarization is adjusted to yield maximal signal modulation depth. The diffraction grating of 1200 lines/mm together with the 100mm focal length achromatic doublet image an optical bandwidth of 230nm on the CCD (ANDOR H1024xV250, 1MHz ADC, fast kinetics mode) with a spectral resolution of 0,22 nm. With this resolution the covered depth range in air amounts to 700 µm. With a beam diameter of 5mm at the entrance of the spectrometer, we calculate a beam waist at the CCD of 21µm, which is covered by the CCD pixel size of 25µm x 25µm. The CCD camera records a set of 160 lines with an acquisition rate of 10000 equivalent A-scans per second. After such data block is acquired the data is digitized and transferred to the host computer. The recording of a tomogram of 160 x 512 pixels is as fast as 16ms however the repetition rate for recording the tomogram blocks is only 4 Hz. The duty cycle of the current system is therefore only 6.4%. This number can significantly be improved by using a larger buffer size and a faster analog-to-digital conversion board (ADC board) [12,14,17]. A block size of 160 A-scans was chosen to realize real time imaging for adjustment of the measurement head relative to the volunteer eye with 4Hz block tomogram rate. The rate would have been much slower in case of exploiting the full 250 lines of the CCD head. The acquired data is processed and displayed using specially developed software (LabView; National Instruments Inc.). The software post-processing time including resampling and Fourier transform for a tomogram of 1000 x 512 pixels needed 0,6s on a host computer equipped with a Pentium IV 2GHz processor.

2.2 Theory

The principle of FD OCT relies on the fact that the spectral amplitude of the backscattered light equals the Fourier transform of the longitudinal sample structure. Hence inverse Fourier transform of the measured intensity yields the autocorrelation of the object function. Actually one obtains the cross correlation between sample and reference arm light as well as the auto-correlation terms of both arms individually. In case of strongly reflecting or backscattering samples, the latter terms might significantly obscure the true sample structure that is given by the cross correlation terms. Sophisticated phase shifting methods to extract the complex signal allow for a complete removal of those terms [7,18,19]. For retinal imaging however it was shown to be sufficient to subtract the reference arm signal to achieve shot noise limited and autocorrelation free imaging [6]. The main advantage of FDOCT lies in the fact that one full depth scan is obtained synchronously. The Fourier transform itself acts as a band pass filter with a width of 2/*N*, where *N* is the number of CCD pixels, i.e., the spectral sampling points. This is due to the fact, that each modulation frequency of the spectrum corresponds to exactly one Fourier bin in the positive and one in the negative frequency range. For this reason, FD OCT has a large sensitivity advantage as compared to time domain OCT where the electronic band pass width depends on the depth scanning speed and optical bandwidth of the employed light source. The benefit of FD OCT is, that data acquisition time can be improved by a factor of 50 or more without loosing sensitivity in comparison to TD OCT applying the same optical power to the sample.

The maximal achievable depth range $z_{\max}$ is determined by the spectrometer resolution $\delta\lambda$ and the center wavelength λ_0 according to $z_{\max} = \lambda_0^{\,2}/(4\delta\lambda)$. The number of sampling points within this depth range is given by half the number of CCD pixels as a result of the discrete Fourier transform. Assuming that the full spectrum of the light source is imaged onto the CCD, the axial resolution δz is equal to half of the coherence length, i.e., $\delta z = (2\ln 2/\pi)\lambda_0^{\,2}/\Delta\lambda$, where $\Delta\lambda$ is the full width half maximum of the light source's spectrum. The coherence function acts therefore as a point spread function for the reconstructed object structure, its full width half maximum spans over $n_{\Delta z} = (N/2)\,\delta z / z_{\max}$ sampling intervals. In the present case the wavelength dependence of the fiber coupler, fiber collimators, and residual chromatic aberration of lenses caused a shift of the center wavelength to λ_0=820nm [see Fig. 2(a)]. With N=1024, $\Delta\lambda = 100$nm, and $z_{\max}$~700µm a depth resolution in air of 3µm and a sampling of $n_{\Delta z}$~ 3 points was calculated.

#4012 - $15.00 US Received 11 March 2004; revised 28 April 2004; accepted 3 May 2004

2.3. Dispersion and resolution

As already mentioned the recorded interference signal is a function of wavelength rather than time. In the case of a single reflecting surface in the sample arm it is of the general form

$$I(\lambda) = I_r(\lambda) + I_s(\lambda) + 2\sqrt{I_r(\lambda)I_s(\lambda)}\cos(2f(\lambda)\Delta z + g(\lambda)), \qquad (1)$$

where $I_{r,s}$ is the intensity of the reference and sample arm light respectively, and Δz is the relative optical path length between both arms. The functions $f(\lambda)$ and $g(\lambda)$ are crucial as they determine the system resolution. They will be described in more detail in the following paragraph.

In general one needs to Fourier transform the backscattered intensity as a function of wavenumber K or frequency ν in order to reconstruct the associate time domain depth profile. Ideally $g(\lambda)$ is only an arbitrary phase constant that can be neglected without loss of generality, and $f(\lambda) = K = 2\pi/\lambda$. Assuming however a dispersion mismatch between both arms associated with a material thickness d, $g(\lambda)$ will no longer be constant but of the form $g(\lambda) = 2d\, f(\lambda)\,(n(\lambda)-1)$, where $n(\lambda)$ is the wavelength dependent refractive index of the dispersive material. It is well known that the dispersion $dn(\lambda)/d\lambda$ and higher order terms cause a broadening of the coherence envelope, therefore the dispersion mismatch between reference and sample arm needs to be minimized to achieve optimal depth resolution. Especially in the case of retinal imaging one also needs to compensate for the dispersive ocular media that the light double passes on its way to the retina and back to the detector [20].

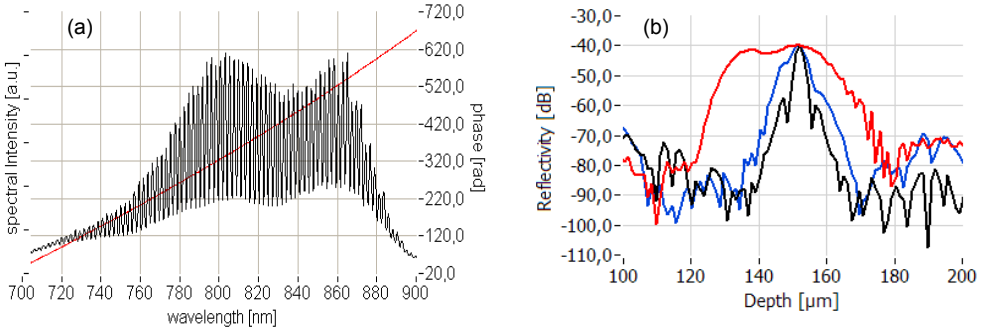

Fig. 2. (a) recorded spectrum (black line) with dispersion and associated signal phase (red line). (b) Time domain signal after FFT without (black line) and with resampling (red line) of the recorded spectrum. The blue line shows the coherence envelope after the coordinate change $\lambda \rightarrow K$.

In order to minimize $g(\lambda)$ one needs to balance the dispersion mismatch between both interferometer arms as explained in section 2.1. Once $g(\lambda)$ has been optimized we are still left with $f(\lambda)$, which describes a non-linear phase as a function of wavelength λ in the cosine term of Eq. (1). This non-linearity causes an additional broadening of the coherence envelope after discrete Fourier transform (DFT) of Eq. (1). Apart from the relation $\lambda \leftrightarrow$K it is due to dispersion of the diffraction grating, imaging errors of the lens in front of the CCD, misalignment, finite CCD pixel sizes, or surface imperfections of the optics. The actual non-linear phase function needs to be resampled to provide equally spaced interference fringes. Fig. 2(a) shows a recorded spectrum of a dispersion balanced FDOCT system with a sample reflectance of -40dB. The plotted phase function (red line) deviates slightly from the ideal linear relation. The phase function was extracted by detecting the fringe peak positions and taking into account that the phase change between two maxima is 2π. A cubic spline interpolation scheme yields all intermediate points. This function was subsequently used to calculate the new sampling points that correct the recorded interference fringes to be equally

#4012 - $15.00 US Received 11 March 2004; revised 28 April 2004; accepted 3 May 2004

spaced. In Fig. 2(b) the logarithmic coherence envelope after DFT of the modulated spectrum is shown for the original non-linear interference pattern (red line) and for the resampled pattern (black line). The blue line in Fig. 2(b) shows the coherence envelope if only a coordinate change in the spectrum from wavelength to wavenumber was performed [6]. One recognizes a residual non-linearity due to the factors that are mentioned previously that causes a broader coherence envelope as compared to that obtained with the resampling technique. It is obvious, that already a small non-linearity causes a significant decrease of depth resolution. After the correction a resolution in air of 3µm was achieved that decreased to 3,7µm at the far end of the depth range. This corresponds to 2,3µm to 2,8µm in tissue respectively (n=1,35). The resolution loss is a result of the finite pixel width of the spectrometer. Due to the recorded chirped interference pattern there will be always higher frequencies at one end of the modulated spectrum. Those appear with a reduced modulation depth as will be explained in the next section. Hence the effective spectral width for the FD OCT signal is reduced which results in a resolution loss for structures which are closer to the maximal depth position.

2.4. Sensitivity and dynamic range

Recently it was theoretically stated and experimentally verified, that FD OCT systems including swept source FD OCT possess a large sensitivity advantage as compared to TD OCT systems [7-11]. One can attribute the increased sensitivity to the smaller effective electronic bandwidth that is independent from depth scanning range and depth scanning velocity. Nevertheless due to the finite pixel size of the array detector in the case of FD OCT there is a modulation depth loss as one records higher frequencies. After DFT, this corresponds to a sensitivity decay as one approaches the maximal depth position, as was shown by Leitgeb *et al.* [9], and refined by Yun *et al.* [13]. In the present case the sensitivity decreased from 94 dB to about 87dB across the full depth range.

Another important issue is dynamic range (DR), which is limited by the saturation of the CCD detector. In practice the DR depends on the level of the reference arm power that is set close to the saturation level in order to achieve maximal sensitivity. To analyze the dynamic range, the reference arm light is assumed to be $N_{ref}=\gamma N_{sat}$, where $0<\gamma<1$, and N_{sat} is the number of photoelectrons that saturate one camera pixel. The maximal sample signal $N_{s,max}$ can be calculated from the condition that the recorded interference pattern maximum should not exceed the saturation value, i.e., $N_{sat}=N_{s,\max}+N_{ref}+2\sqrt{N_{s,\max}N_{ref}}$. Solving this equation for $N_{s,max}$ results in $N_{s,\max}=N_{sat}\left(1+\gamma-2\sqrt{\gamma}\right)$ [Fig. 3(a)]. The dynamic range (DR) at a given reference arm power setting can be assumed to be the ratio of maximal to minimal OCT signal. The signal to noise ratio (SNR) in the shot noise limit with $N_{ref} >> N_s$ can be written as $SNR = N N_s$ [9]. With a signal to noise ratio (SNR) of two for the minimal signal one obtains:

$$DR=\frac{N_{sample}^{\max}N_{ref}}{N_{sample}^{\min}N_{ref}}=\frac{N_{sat}\gamma\left(1+\gamma-2\sqrt{\gamma}\right)}{2/N}. \qquad (2)$$

The number of photoelectrons at the signal peak is approximated as 1/N times the total number across the entire array. The situation is plotted in Fig. 3(b). Note that the values represent the DR and should not be misinterpreted as sensitivity figures. In a typical situation of γ=0.7 we expect a DR of about 65dB. The strongest peak in retinal tomograms corresponds to the retinal pigment epithelium (RPE) with a reflectivity of about -50dB. Given a typical sensitivity of 90dB one would be able to detect structures with reflectivities of 40dB below the RPE reflectivity which lies well within the dynamic range. This range might however be significantly reduced by incoherent backscattered light especially from cornea and lens. One can include this effect into Eq. (2) by calculating $N_{s,\max}=N_{sat}\left(\gamma+(1-\xi)-2\sqrt{\gamma(1-\xi)}\right)$, where ξ is the ratio of incoherent light intensity to the saturation value. Fig. 3(b) shows the effect of incoherent background signal to the DR.

#4012 - $15.00 US Received 11 March 2004; revised 28 April 2004; accepted 3 May 2004

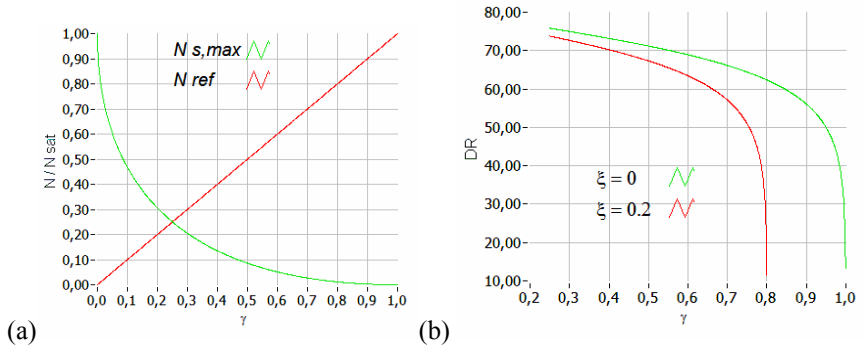

(a) (b)

Fig. 3. (a) dependence of $N_{s,max}$ and N_{ref} to the load factor γ. (b) Dynamic range in the shot noise limit without (ξ=0) and with (ξ=0.2) incoherent background (N_{sat} = 300 k e$^-$, N=1024).

The calculations show that even in the presence of a strong incoherent background the dynamic range is sufficient to exploit the high sensitivity of FD OCT for retinal imaging.

One might ask why TD OCT systems that employ Ti:Sapph lasers to achieve ultrahigh resolution imaging need balanced detection to eliminate random intensity noise (RIN) and to achieve shot noise limited detection, whereas FD OCT systems do not. If one writes the RIN in the case of FD OCT for unpolarized light as N_{sat}^2 N /(2 $\Delta\nu_{eff}$ τ) one obtains for the ratio between shot noise and RIN per pixel Q = 2 $\Delta\nu_{eff}$ τ / N_{sat}., where $\Delta\nu_{eff}$ is the effective line width and τ the exposure time [7]. From the plot of this relation in Fig. 4 one can verify that for 100µs exposure time shot noise dominates over RIN. Only for equivalent A-scan rates of 200kHz corresponding to 5µs exposure time, RIN starts to be the dominant contribution and balanced detection will be necessary to maintain the shot noise limit for FD OCT. Note that due to the high sensitive CCD camera the reference arm power incident on one pixel with 100µs exposure time is only ~2nW, which is some orders smaller than usual reference powers detected in TD OCT.

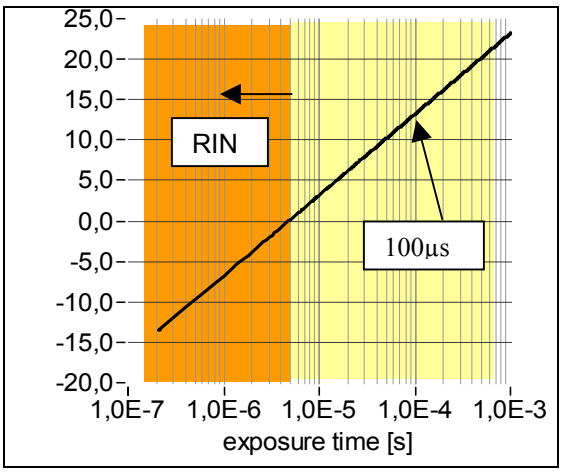

Fig. 4. Relation of shot noise to RIN. (N_{sat} = 400 ke-, λ_{cent}=820nm, FWHM=100nm, N=1024).

#4012 - $15.00 US
Received 11 March 2004; revised 28 April 2004; accepted 3 May 2004

3. Results and discussion

All subsequent measurements were performed using the resampling technique described above. The sensitivity of the FD OCT system was 90 dB with an illumination time of 100µs and a power of 300µW at the sample. In a first step a polyethylene- terephthalat (PET) foil (n=1,6) of 3µm thickness was measured to demonstrate the resolution of the FDOCT system. Fig. 5(a) shows a single depth scan and simple DFT of the recorded and processed spectrum. As mentioned above, with the current setup there are only ~3 sampling points to resolve the FWHM of the coherence envelope. For a precise thickness measurement a zero padding technique was applied to increase the sampling density in the time domain by a factor of ten as displayed in Fig. 5(b). The two peaks corresponding to front and back surface of the foil are clearly distinguished.

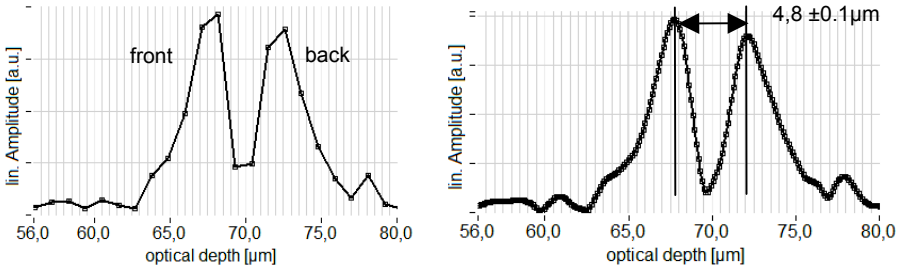

Fig. 5. Effect of spectral zero padding to increase sampling point density in the time domain. The values shown on the x-axes are optical path lengths.

Cross-sectional measurements were performed across the foveal region of the human retina of two healthy subjects in vivo, where a set of blocks of 160 spectra was recorded. They correspond to tomograms of 160 horizontal and 512 depth pixels. Hence a tomogram of 1280 lines consist of 8 blocks that need a recording time of 2 seconds whereas each individual block is recorded in only 16ms. They can be regarded as being free of moving artifacts. The residual artifacts due to eye movements during the read out of the data blocks are easily corrected manually by lining up the tomogram blocks after the post processing algorithms. In Fig.6 the performance of the ultrahigh resolution FD OCT system as compared to that of a time domain system is demonstrated using the same light source. The ultrahigh resolution TD OCT tomogram consists of 600 points and is recorded with up to 250 A-scans per second and a power of 800µW at the cornea. The FD OCT tomogram shown in Fig. 6.a consists of 1150 transversal points. The visualization of intraretinal layers seems to be better in case of FD OCT in the region of the photoreceptor layer, especially the inner and outer segment of the photoreceptor layer, which might be due to the higher transverse sampling rate of ultrahigh resolution FDOCT as well as possible motion artifacts present in the TD OCT image. In both cases the external limiting membrane can be resolved and may be used for a quantification of the photoreceptor layer thickness [21]. The sensitivity of the proximal retinal structures is reduced in case of FD OCT as a result of the sensitivity loss across the depth as explained in sec. 2.4. From the magnified regions one clearly recognizes that all intraretinal structural details that are visible in the TD OCT tomogram are comparably present in the FD OCT image.

A limitation of the current system is the small depth range of ~700µm that makes it difficult to adjust the volunteer's relative distance to match the coherence range. This is also the reason why the whole pigment epithelium is not visualized across the entire tomogram. The structure already appears at a position close to the origin of the depth range. One can easily enhance the depth range without reducing the sampling density by using a camera head with more horizontal pixels.

#4012 - $15.00 US Received 11 March 2004; revised 28 April 2004; accepted 3 May 2004

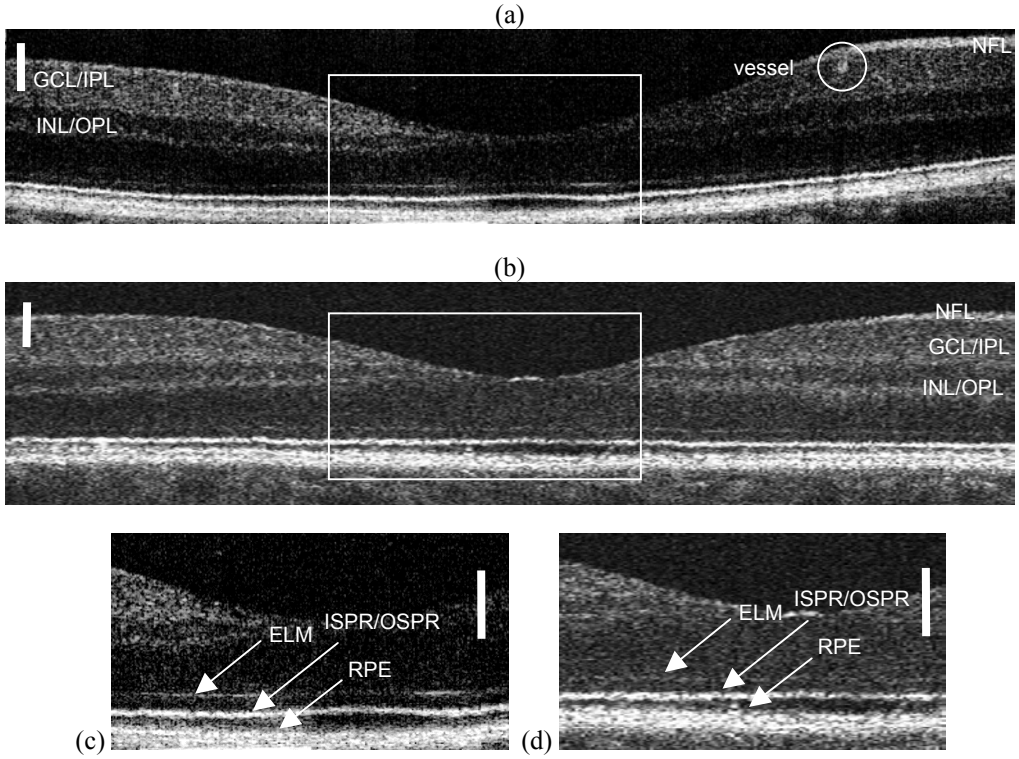

Fig. 6. (a) Ultrahigh resolution by Fourier Domain optical coherence tomography with 10 kHz A-scan rate, 300µW at the sample, and 3µm axial resolution in free space across the foveal region of the retina. (b) Comparison to time domain optical coherence tomography with 130 Hz A-scan rate, 800µW at the sample, and ~3µm axial resolution in the retina. (c) Enlarged section of (a). (d) Enlarged section of (b).The imaged eyes are of different healthy volunteers. The white scale bars represent 100µm. The tomograms in (a) and (b) spread over ~5mm laterally, the sections in (c) and (d) over ~1,5mm. No image processing was applied. (NFL, nerve fiber layer; GCL, ganglion cell layer; IPL/OPL, inner/outer plexiform layer; INL, inner nuclear layer; ELM, external limiting membrane; ISPR/OSPR, inner/outer segment photo receptor layer; RPE, retinal pigment epithelium.)

4. Conclusions

For the first time *in vivo* ultrahigh resolution images (~2.5µm) obtained with Fourier domain OCT are presented and compared to images that are taken with an ultra high resolution time domain OCT system. They show comparable performance though the acquisition speed for the single lines is at least 40 times higher in case of FD OCT. Additionally there is considerably less data necessary for recording the full fringe interference pattern. The system is currently limited by the buffer size of the camera which will be changed in the future to increase the duty cycle of the system. Main advantages of using FD OCT for high resolution biomedical imaging are its acquisition speed that minimizes motion artifacts as well as the smaller amount of data that would ultimately allow for an effective three dimensional imaging of biologic tissue with ultra high resolution. Morphological features at the cellular level might be of great clinical importance to improve the early diagnosis and the assessment of tissue pathologies. As ultrahigh resolution provided a quantum leap in visualization performance FD OCT additionally pushes OCT performance forward to allow also for high acquisition speed and three dimensional imaging.

#4012 - $15.00 US Received 11 March 2004; revised 28 April 2004; accepted 3 May 2004

Acknowledgment

We acknowledge the Austrian National Bank (Jubilaeumsfonds grant Nr. 9654), the Austrian Academic Exchange Service OEAD together with the Polish State Committee for Scientific Research (grant 2003/13), the Austrian Fonds zur Foerderung von Wissenschaft und Forschung (FWF grants P14529-PSY, P14218-PSY), and the CRAFT program (CRAF-1999-70549) for their financial support. We thank Carl Zeiss Meditec Inc. for providing the OCT system and Femtolasers GmbH for the Integral Femtosource Integral OCT.

#4012 - $15.00 US Received 11 March 2004; revised 28 April 2004; accepted 3 May 2004